Isothermal Crystallization of Hydrogenated Sunflower Oil: II. Growth and Solid Fat Content

M.L. Herrera[a,*], C. Falabella[b], M. Melgarejo[b], and M.C. Añón[a]

[a]Centro de Investigación y Desarrollo en Criotecnología de Alimentos (CIDCA) (UNLP-CONICET), Provincia de Buenos Aires, Argentina, and [b]Molinos Río de La Plata S.A. Buenos Aires 1323, Argentina

ABSTRACT: Isothermal crystallization of sunflower seed oil hydrogenated under two different conditions was studied by means of pulse nuclear magnetic resonance (pNMR) and optical microscopy. Solid fat content (SFC) curves showed two different shapes depending on supercooling. When supercooling was high, hyperbolic curves were found, whereas with low supercooling sigmoidal curves were obtained. Curves were interpreted with the modified Avrami equation. Photographs of the crystals were taken from the beginning of crystallization, every 15 s until 15 min and every 5 min until 60 min. Samples which exhibited hyperbolic curves showed a slight increase in crystal number, and crystals were needle-shaped in all cases. Samples which had sigmoidal crystallization curves showed a marked increase in crystal number with time, and crystals were spherical in shape. Crystallization behavior was also in agreement with the chemical composition of the samples. Samples which had the highest content of high-melting triacylglycerols (especially trielaidin) showed only hyperbolic curves. Supercooling is a very important parameter that defines the way nucleation occurs. Depending on the initial number of nuclei, two different growth mechanisms were found: a uniform linear growth of the nuclei for a small initial number (sigmoidal curves) and an aggregate of the nuclei for a high initial number (hyperbolic curves).

Paper no. J8635 in *JAOCS 76*, 1–6 (January 1999).

KEY WORDS: Avrami equation, crystal growth, hydrogenated sunflower seed oil, isothermal crystallization, solid fat content.

The functional performance and textural quality of fats and the products containing them are mainly determined by the balance between solid and liquid phases and the crystal structures of the fat solids (1). The measurement of solids over a range of temperatures is utilized by the industry to evaluate the plastic temperature interval of fats and oils.

Crystallization can generally be classified in two steps: nucleation, followed by crystal growth. As a crystal starts to grow, the difference in chemical potential between a molecule in the solution and one at a site in the crystal will determine the growth rate. This difference is directly related to the supercooling of an oil or the supersaturation of a solution (2). The growth process of a fat crystal is important in technical processing. In some processes, fats should be completely crystallized by the end of the production line. For example, if the percentage of crystallization reached after 1 h is half of the final crystallization, this means that during the technical processing of fats, crystallization equilibrium will not be reached. Therefore, standard processing times used for fats which completely crystallize in an hour should be modified (3).

Six main triacylglycerols are present in sunflower seed oil. When this oil is hydrogenated, geometrical and positional isomers are formed and the resulting oil is a very complex system (4). Previous investigations on crystallization of hydrogenated oil focused mainly on polymorphism and intersolubility of the crystals by means of differential scanning calorimetry, X-ray diffraction, microscopy and laser-polarized light turbidimetry techniques (4,5). The fractionation process and the effects of various processing conditions, such as different thermal treatments and rates of cooling on crystallization behavior, were also investigated (6–8).

The aim of this work is to study the isothermal crystallization behavior of sunflower seed oil hydrogenated under two different conditions. Measurements of its solid fat content by nuclear magnetic resonance (NMR) and a description of the growth behavior in terms of number and size of the crystals formed are reported.

MATERIALS AND METHODS

Starting oils. Sunflower seed oil was hydrogenated as was previously indicated (4). Two different hydrogenation conditions were selected: (i) high temperature of reaction and low pressure of hydrogen gas (190°C, 1 kg/cm^2), and (ii) low temperature and high pressure (170°C, 2.5 kg/cm^2). The studied samples were samples 6, 7, and 8 from the first hydrogenation process and samples 14, 15, and 16 from the second hydrogenation process (4). Dropping points of the samples were determined with the Mettler FP 80 Dropping Point Apparatus (Mettler Instruments A.G., Greifensee-Zurich, Switzerland), using a heating rate of 1°C/min. The solid fat index (SFI) of the samples was determined by dilatometry using the cooling methods of AOCS method Cd-57 (9), which consists of heating the fats to 60°C, solidifying at 0°C for 15 min, tempering at 26.7°C for 0.5 h, cooling again at 0°C for 15 min, and then

*To whom correspondence should be addressed at CIDCA, Casilla de Correo 553 (1900) La Plata, Provincia de Buenos Aires, Argentina. E-mail: mcanon@isis.unlp.edu.ar

measuring the SFI after conditioning for 0.5 h at the appropriate temperatures. These results, as the Mettler dropping points, are shown in Table 1.

NMR. SFC of the samples were measured by pulsed nuclear magnetic resonance (pNMR) in a Minispec PC/120 series NMR analyzer (Bruker, Karlsruhe, Germany). The number of hydrogen nuclei in the liquid and the total number of hydrogen nuclei in liquid and solids were measured. The percentage of solid content is given by the following equation:

$$S(\%) = \frac{(SA_1 - SA_2)F}{(SA_1 - SA_2)F + SA_2} \times 100 \quad [1]$$

where SA_1 is the signal amplitude proportional to the total number of hydrogen nuclei, SA_2 is the signal amplitude proportional to the hydrogen nuclei in liquid, and F is a factor to correct the dead-time of the receiver since it is not possible to measure the samples at time zero. F was previously determined by using standards with a known percentage of solids. Samples were run in triplicate and the values were averaged. The SFC of the samples was determined using the following thermal treatment: samples were melted at 80°C for 30 min, and then the NMR tubes were filled with the samples and placed into a bath at crystallization temperature. Selected crystallization temperatures were 20, 15, 10, 6, and 3°C. SFC was measured as a function of time. The obtained curves were fitted with the modified Avrami equation as described in the Results and Discussion section. An X-Y table was made for every experimental curve with the solid content and the corresponding time ($n = 3$). To obtain the parameters which gave the best fit, the nonlinear section of the Systat method was used (Systat, Inc., Evanston, IL). The software calculated them using the selected model and the experimental data of the X-Y tables. Means are reported in Tables 2 and 3, including the quadratic error to indicate the goodness of the fit. Linear regressions ($n = 1$) were fitted with Microsoft Excel 7.0 for Windows (Microsoft, Redmond, WA) software. Results are reported in Tables 2 and 3. Statistical significance of differences in parameters S_{max} (obtained from Figs. 1 and 2) and K_n, with supercoolings and between samples, was checked using analysis of variance. A randomized block design and an additive model which assumes that an observation, γ_{ti}, can be represented as the sum of a general mean η, a block effect β_i, a treatment effect τ_t, and an error ε_{ti}, were selected. A multiple comparisons test was used to determine the confidence interval for a particular difference in means.

Optical microscopy. A Leitz microscope model Ortholux II (Ernest Leitz Co., Wetzlas, Germany) with a controlled-temperature platform was used to follow crystallization. In the crystallization tests, the samples were melted at 80°C and held at this temperature for 30 min. Samples were then placed on the slide at crystallization temperature and covered with a cover slip. The platform temperature was controlled by a Lauda TUK cryostat (Werklauda, Königshofen, Germany), which was filled with a mixture of ethylene glycol/water 3:1 (vol/vol). Photographs of the crystals were taken with a Leitz-Vario-Orthomat camera under polarized light during crystallization from the beginning, every 15 s until 15 min and every 5 min until 60 min. The photographs was scanned with a Genius Color Page CS scanner (KYE Corporation, Torrance, CA); the number of crystals were determined using ImagePals 2 version 2.0 software. These data were evaluated with Microsoft Excel 7.0 for Windows software to obtain the crystal size distribution. Crystal size was arbitrarily considered as the longest dimension of the crystal (the diameter for spherical shape crystals and the length for needle shape crystals).

RESULTS AND DISCUSSION

Crystallization curves by SFC. Figures 1 and 2 show the solid fat content vs. time of crystallization for samples 14–16 and 6–8, respectively. Samples 15 and 16 (Fig. 1) showed hyperbolic curves for all temperatures. Crystallization initially was fast. At all temperatures, there was no induction time of crystallization for either sample and therefore no step was observed in solid fat vs. time curves even at 20°C. The maximum SFC (S_{max}) of all samples were in agreement with their Mettler dropping points, except for sample 14, which exhibited a slightly lower S_{max} than expected. Samples 6, 7, 8, and 14 (Fig. 2) showed sigmoidal curves at 20°C. Sample 6 also showed this shape at 15°C for the SFC over time. That is, there was an induction time with no fat crystallization, followed by a period of faster crystallization. For the other temperatures, samples 6, 7, 8, and 14 also showed hyperbolic curves.

Mathematical interpretation. To describe the curves in Figures 1 and 2, the modified Avrami equation was used. This

TABLE 1
Mettler Dropping Point and Solid Fat Content of Samples

		Solid fat index (%)				
Sample	Mettler dropping point (°C)	10°C	21°C	27°C	33°C	38°C
16	40.4	45.4	32.4	26.7	15.1	5.9
15	36.8	37.6	22.9	16.2	6.2	0.6
14	32.4	30.1	14.9	7.7	1.4	—
8	33.8	38.5	21.8	13.4	3.4	—
7	32.2	33.1	16.9	8.4	0.8	—
6	30.3	27.4	12.3	4.7	—	—

TABLE 2
Nuclear Magnetic Resonance (NMR) Curves Fitted by the Modified Avrami Equation[a]

Temperature (°C)	n	K_n (min^{-1})	r^2
Sample 16			
20	1	0.209	0.934
15	1	0.283	0.953
10	1	0.293	0.980
6	1	0.321	0.955
3	1	0.303	0.988
Sample 15			
20	1	0.137	0.935
15	1	0.216	0.998
10	1	0.316	0.965
6	1	0.315	0.994
3	1	0.294	0.988
Sample 14			
20	3	0.025	0.986
15	1	0.136	0.983
10	1	0.310	0.967
6	1	0.338	0.945
3	1	0.284	0.986

[a]$-\ln(1 - f) = (K_n t)^n$ where n is an integral number, t is time, K_n is the rate constant, and f is the fractional crystallization.

equation is based on three-dimensional random nucleation, followed by a uniform linear growth of the nuclei. It is:

$$-\ln(1 - f) = (K_n t)^n \quad [2]$$

where $n = 3$ or 4 and represents the index of the reaction; t is time; K_n is the rate constant; and f is the fractional crystallization. The value of n is an integral number. Samples 6, 7, 8, and 14, crystallized at 20°C, and sample 6, crystallized at 15°C, were evaluated using this model with $n = 3$. The rate constants are shown in Tables 2 and 3. As can be observed from these tables, the SFC data fit the equation well over the rate of fractional crystallization from 0 to 0.7 ($r^2 > 0.9$ in all cases). Sample 8 had the highest rate constant, followed by sample 7 and then sample 6. The rate constant of sample 14 was close to that of sample 7.

TABLE 3
NMR Curves Fitted by the Modified Avrami Equation[a]

Temperature (°C)	n	K_n (min^{-1})	r^2
Sample 8			
20	3	0.037	0.995
15	1	0.136	0.968
10	1	0.154	0.962
6	1	0.266	0.951
3	1	0.258	0.989
Sample 7			
20	3	0.026	0.989
15	1	0.163	0.957
10	1	0.111	0.982
6	1	0.240	0.990
3	1	0.232	0.967
Sample 6			
20	3	0.008	0.963
15	3	0.022	0.976
10	1	0.134	0.937
6	1	0.201	0.993
3	1	0.209	0.957

[a]See Table 2 for equation and abbreviations.

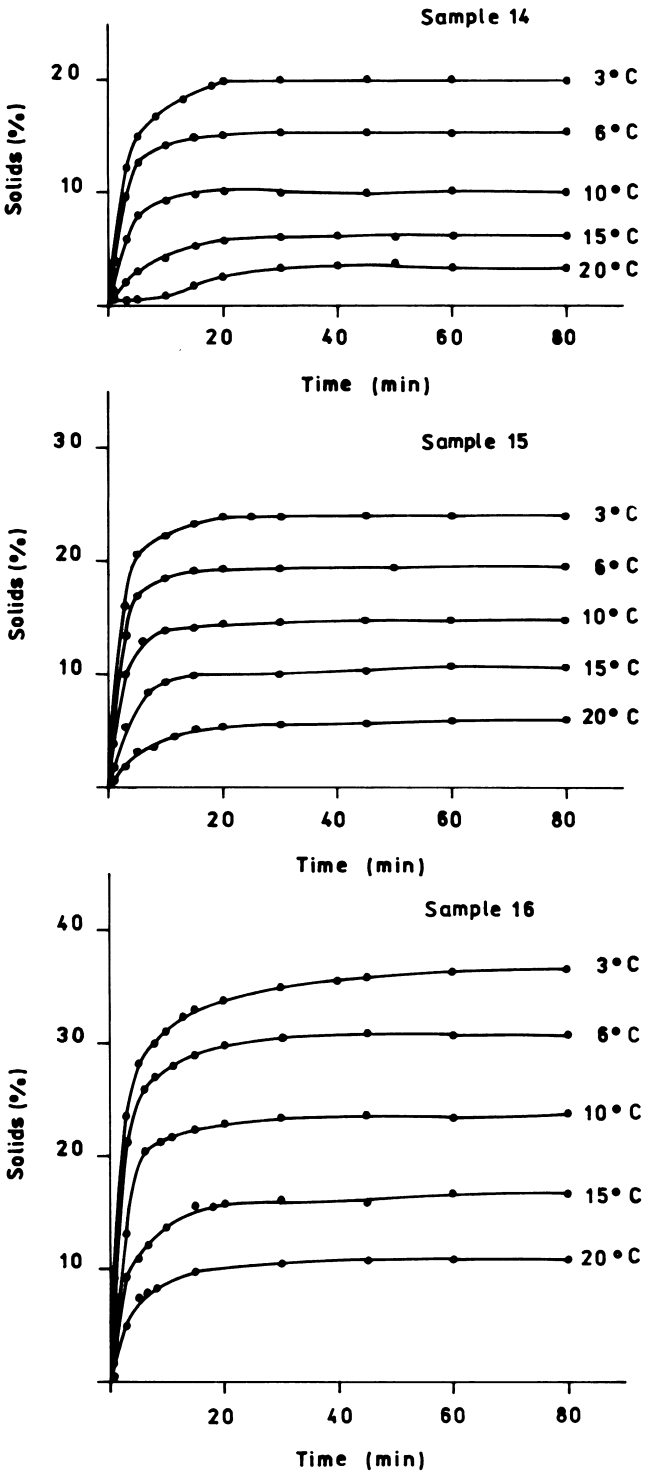

FIG. 1. Solid fat content vs. time of crystallization for samples 14, 15, and 16 (first hydrogenation).

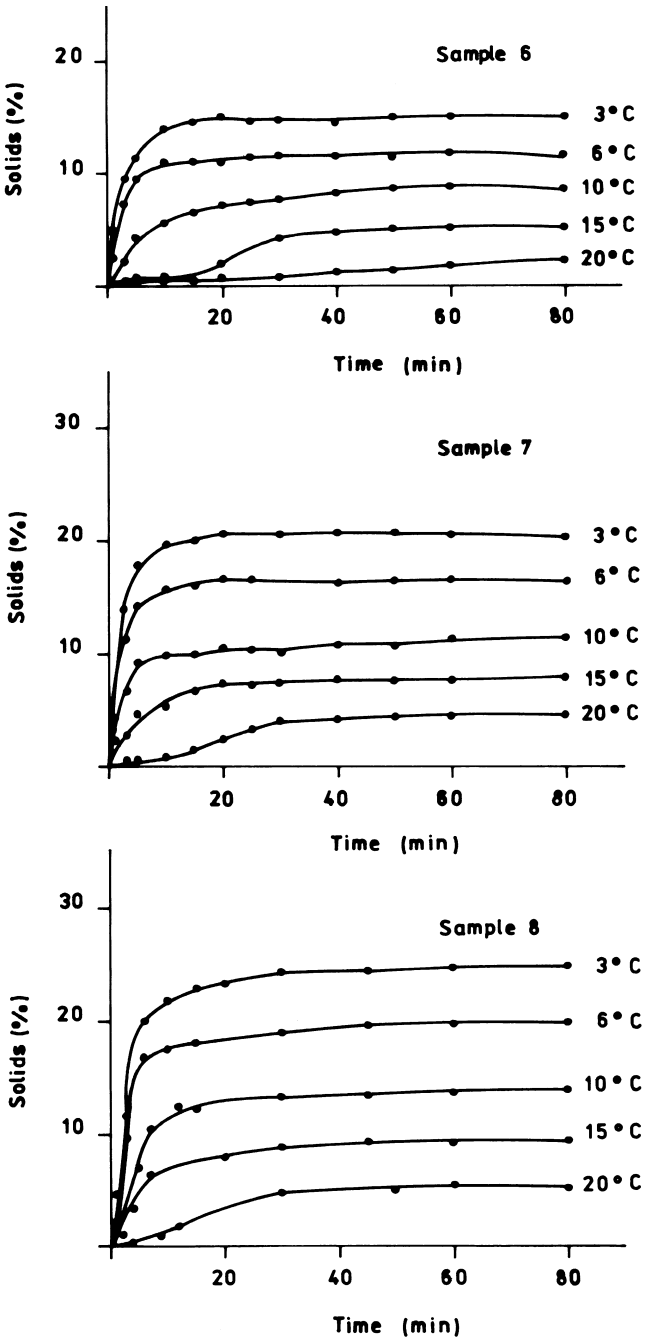

FIG. 2. Solid fat content vs. time of crystallization for samples 6, 7, and 8 (second hydrogenation).

Hyperbolic curves can also be described by the modified Avrami equation but in this case n should set to 1. The resulting equation is an exponential growth curve, which is similar to a hyperbolic curve. Tables 2 and 3 show the values of K_n and the correlation coefficients for samples 16, 15, and 14 (second hydrogenation process) and 8, 7, and 6 (first hydrogenation process), respectively. There was also a good fit over the same rate of fractional crystallization for hyperbolic curves. However, in data not shown in the tables, correlation coefficients showed a very bad fit for sigmoidal curves when n was 1 (r^2 was between 0.500 and 0.740). K_n values were higher at lower temperatures ($P << 0.001$), which means crystallization rates were higher for lower temperatures. A high statistical significance was found between samples ($P < 0.004$).

An n value of 1 means a different growth mechanism. A mechanism in which nuclei are aggregated to form crystals instead of a linear growth of nuclei mechanism could be proposed in this case.

Number of crystals. Samples 6–8 and 14–16 were photographed as a function of time, and crystal numbers were determined. At 20°C, the number of crystals per field found for sample 16 was 674, 15 s after the sample was placed on the slide, and 728 after 60 min (sample crystal size distributions are reported in Fig. 3). At this supercooling (20.4°C), the number of crystals per field slightly increased with time. Values for sample 15 were 751 and 788 crystals per field for the same times and temperature. The same behavior was found. Sample 14 showed a different behavior. The first viable crystals appeared 4 min and 45 s after the sample was placed. The number of crystals was 124 initially, and 282 and 784 at 7 and 60 min, respectively. In this case there was a marked increase in crystal number. Sample 8 had a number of crystals per field of 481 and 845 at 3 and 60 min, respectively (sample crystal size distribution is reported in Fig. 4). Before 3 min, crystals could not be seen. Sample 7 showed 657 and 919 crystals per field at 4 and 60 min, respectively. These numbers corresponded to the first and last photographs. For sample 6 crystals first appeared at 7 min and the number per field was 98. At 9 min, the number had increased to 179 and by 60 min increased to 651.

The same general behavior was found at all temperatures. For hyperbolic curves, the number of crystals slightly increased from the beginning of crystallization to 60 min. Sigmoidal curves showed a marked increase in crystal number, which was very fast at the beginning.

Sample 16 was also crystallized at 15, 10, 6, and 3°C. The crystal numbers at 15 s and 60 min were, respectively: 776, 791; 788, 859; 790, 870; and 796, 882. The number of crystals slightly increased with supercooling. This result was found for all samples.

Crystal size distribution. Figure 3 shows the crystal size distribution as determined 15 s and 60 min after the beginning of crystallization for samples 15 and 16, and 7 min and 60 min for sample 14. It can be noted from Figure 3 that in the crystal size distribution for sample 16, a high number of crystals had 0.50 μm in the major dimension which increased with time as a result of the growth of smaller crystals. Crystals with sizes such as 0.25, 0.75, and 1.00 decreased, whereas crystals with sizes of 1.25 and 1.75 increased. Larger crystals diminished with time. Sample 15 showed a similar behavior but 0.25 μm crystals slightly increased with time. Sample 14 showed a different behavior. It is clear from Figure 3 that the crystals with sizes of 0.25, 0.50, 0.75, 1.75, 2.00, and 2.25 were in the majority. Inter-

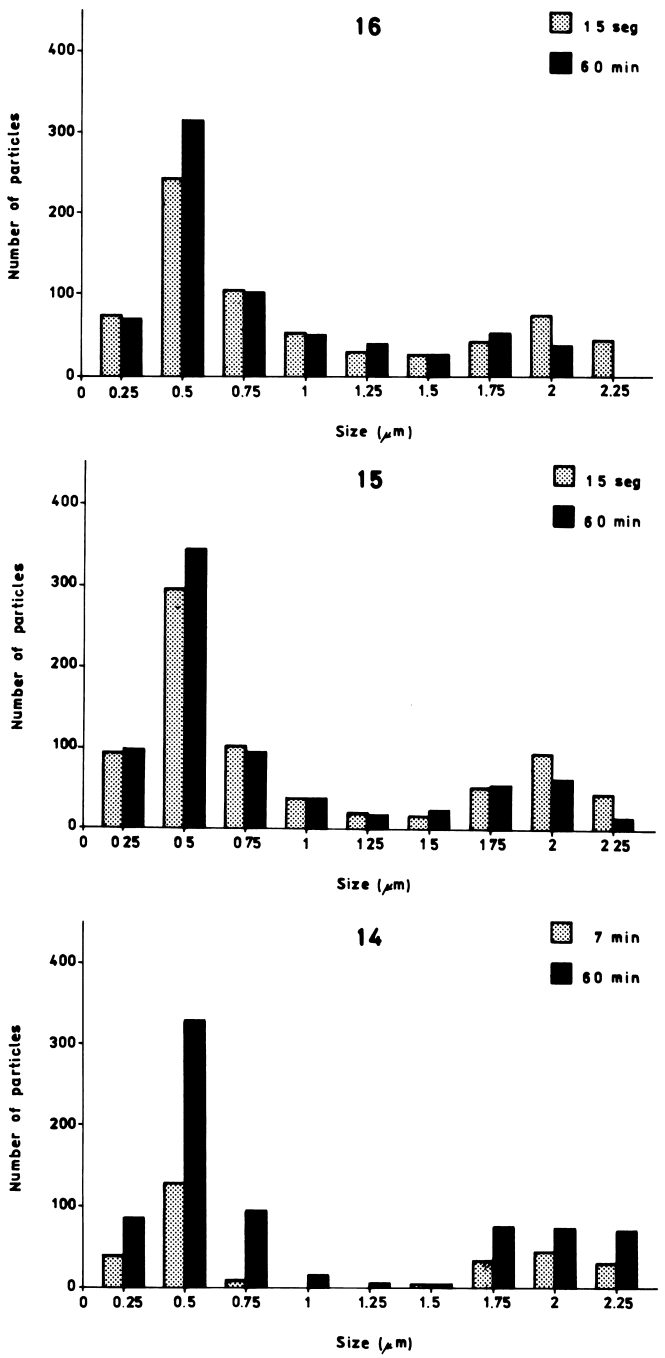

FIG. 3. Crystal size distribution of samples 14, 15, and 16.

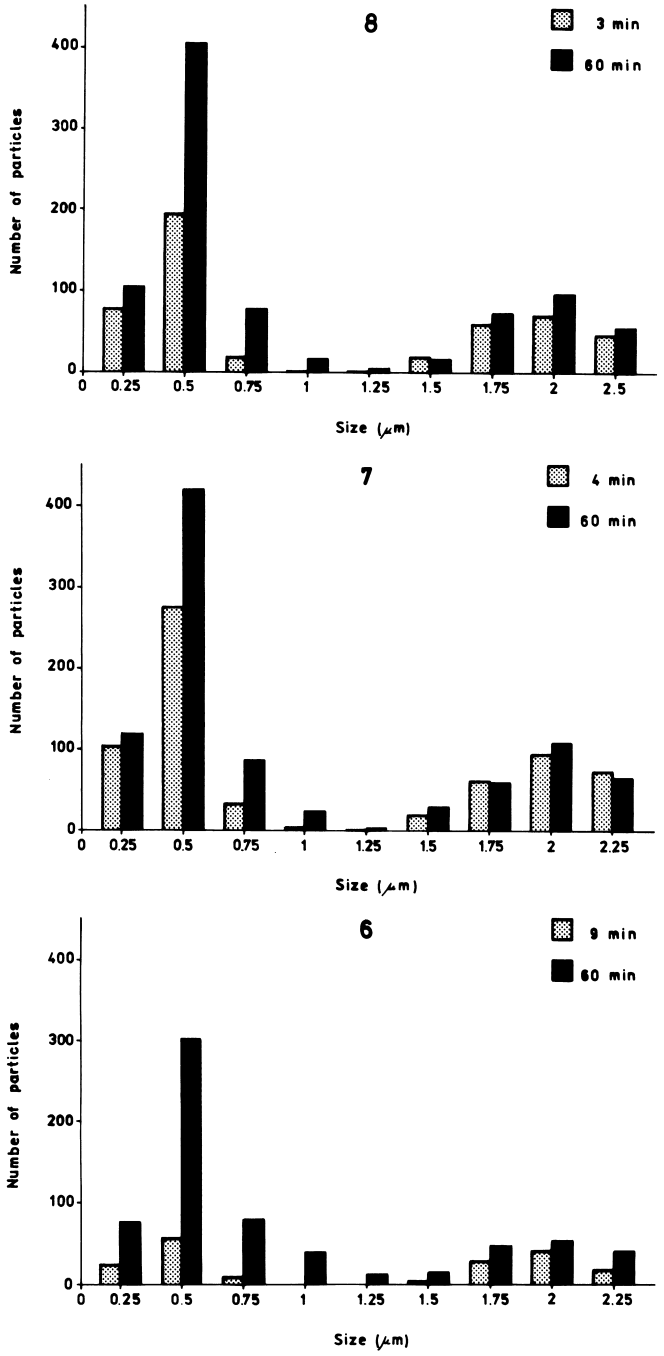

FIG. 4. Crystal size distribution of samples 6, 7, and 8.

mediate sizes such as 1.00, 1.25, and 1.50 were in the minority present.

Figure 4 shows the crystal size distribution of samples 6, 7, and 8 after 9, 4, 3, and 60 min from the beginning of crystallization, respectively. Their distributions were similar to sample 14. Hyperbolic curves showed the behavior reported for samples 15 and 16, and sigmoidal curves demonstrated the same behavior reported for samples 6, 7, 8, and 14. These two behaviors are in agreement with the two different growth mechanisms proposed. The general conclusions for these distributions are that the most important change with time at a crystallization temperature is the increase in crystal number (samples 6, 7, 8, and 14) and the growth of very small crystals up to 0.50 μm (15 and 16).

Sample 16 distribution at different temperatures showed that crystal size was not changed by supercooling. The modes were 0.41, 0.44 at 20°C and 0.40, 0.45 at 3°C for the first and last photograph, respectively. Sample 14 showed mode values of 0.38, 0.39 and 0.30, 0.32 at 20 and 3°C for the first and last photographs, respectively. In the case of S-shape curves, a slight decrease in crystal size was found.

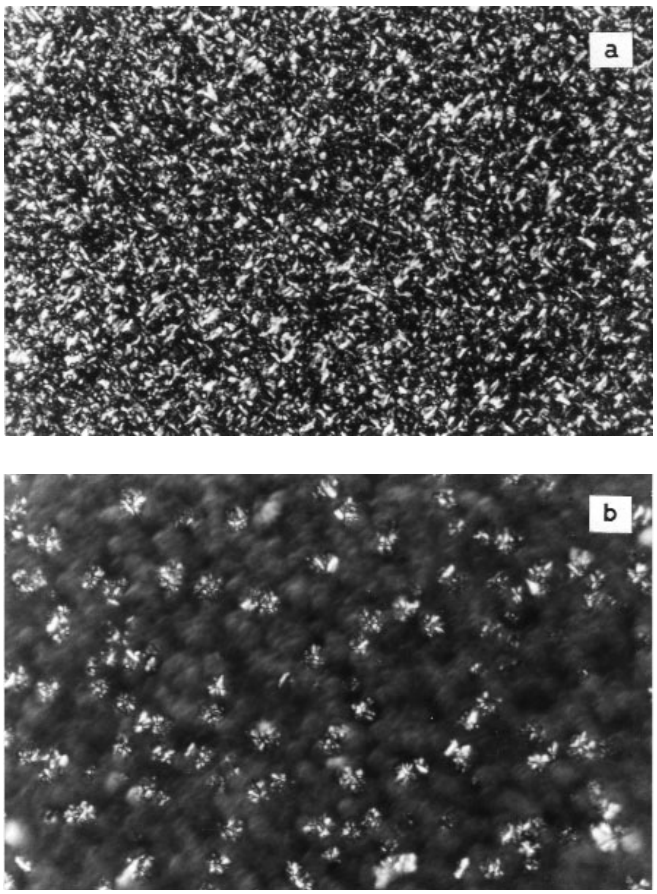

FIG. 5. Morphology of the crystals. (a) Sample 16, crystallized at 20°C, 9 min after having been placed on the slide; (b) sample 6, crystallized at 20°C, 9 min after having been placed on the slide.

Morphology of the crystals. Two different morphologies were found in agreement with the shape of the SFC curves. Samples with hyperbolic curves showed needle-like crystals (Fig. 5a) and samples with sigmoidal curves showed spherical crystals (Fig. 5b).

According to the supercooling, two different crystallization behaviors were found for these samples. When supercooling was high, crystallization started from the beginning, the initial number of crystals was high, and small changes in crystal size were detected with time (hyperbolic curves). On the contrary, when supercooling was low, there was an induction period before crystallization started. Crystallization rate was slow initially and then became more rapid. Crystal number increased significantly with time and a slight change in size was also detected. In this case (sigmoidal curves) there seemed to be a cooperative effect. The first crystals promoted the formation of new ones.

Crystallization behavior was also in agreement with the chemical composition of the samples. Sample 14 and sample 7 had very close Mettler dropping points. As can be observed from Figures 1 and 2, S_{max} values for sample 14 are slightly lower at all crystallization temperatures than values for sample 7. The 95% confidence limit for the mean difference was 1.4, which means these differences have limited statistical significance. However, there is a systematic tendency for SFC values to be lower for sample 14. SFI at 10, 21, and 27°C (Table 1) were also slightly lower for sample 14. These samples had a different chemical composition (4) and therefore different interactions between triacylglycerols could have occurred which could be responsible for the lower obtained values. In addition, samples 15 and 16, which had the highest content of high-melting triacylglycerols (especially OSE and EEE), showed only hyperbolic curves. Samples 6–8, and 14, with lower Mettler dropping points and higher percentages of EEO, showed both behaviors, depending on the supercooling.

Supercooling is a very important parameter which defines the way nucleation occurs. Depending on the initial number of nuclei, two different growth mechanisms were found: a uniform linear growth of the nuclei for a small initial number (sigmoidal curves) and an aggregate of the nuclei for a high initial number (hyperbolic curves).

ACKNOWLEDGMENTS

We are grateful to A. Colavita for expert technical assistance. This work was supported by funds from SECYT (Secretaría de Ciencia y Tecnología) (Prog. Bid 802 OC-AR/Pid 0357), Argentina.

REFERENCES

1. Wan, P.J., Properties of Fats and Oils, in *Introduction to Fats and Oils Technology*, edited by P.J. Wan, American Oil Chemists' Society, Champaign, 1992, p. 32.
2. Larsson, K., Lipids in the Solid State, in *Lipids, Molecular Organization, Physical Functions and Technical Applications*, edited by K. Larsson, The Oily Press, Glasgow, 1994, p. 9.
3. Larsson, K., *Ibid.*, edited by K. Larsson, The Oily Press, Glasgow, 1994, p. 36.
4. Herrera, M.L., C. Falabella, M. Melgarejo, and M.C. Añón, Isothermal Crystallization of Sunflower Oil. I. Nucleation, *J. Am. Oil Chem. Soc. 75*:1273–1280 (1998).
5. Herrera, M.L., Crystallization Behavior of Hydrogenated Sunflower Seed Oil: Kinetics and Polymorphism, *J. Am. Oil Chem. Soc. 71*:1255–1260 (1994).
6. Herrera, M.L., J.A. Segura, and M.C. Añón, Crystalline Fractionation of Hydrogenated Sunflower Seed Oil. I. HPLC Analysis, *Ibid. 68*:793–798 (1991).
7. Herrera, M.L., and M.C. Añón, Crystalline Fractionation of Hydrogenated Sunflower Seed Oil. II. Differential Scanning Calorimetry (DSC), *Ibid. 69*:799–803 (1991).
8. Herrera, M.L., J.A. Segura, G.J. Rivarola, and M.C. Añón, Relationship Between Cooling Rate and Crystallization Behavior of Hydrogenated Sunflower Seed Oil, *Ibid. 70*:898–905 (1992).
9. *Official and Tentative Methods of the American Oil Chemists' Society,* edited by W.E. Link, American Oil Chemists' Society, Champaign, 1974, Method Cd 10-57.

[Received September 5, 1997; accepted September 1, 1998]